

Development of PLZT film-on-foil capacitors with high energy density

Beihai Ma, Manoj Narayanan, Shanshan Liu, Zhongqiang Hu
and Uthamalingam Balachandran

Energy Systems Division, Argonne National Laboratory, Argonne, IL 60439, USA

Email: bma@anl.gov

Abstract. Ceramic thin films with high dielectric constant and high breakdown strength hold special promise for advanced electronics applications. We deposited lanthanum-doped lead zirconate titanate (PLZT) on base metal foils (film-on-foils) by chemical solution deposition. The PLZT film-on-foils were characterized over a wide temperature range between room temperature and 200°C. For $\approx 2\text{-}\mu\text{m}$ -thick PLZT films grown on LaNO_3 -buffered nickel foils at room temperature, we measured a dielectric constant of ≈ 1300 , dielectric loss of ≈ 0.07 , remanent polarization of $\approx 26\text{ }\mu\text{C}/\text{cm}^2$, coercive field of $\approx 29\text{ kV}/\text{cm}$, leakage current density of $\approx 9.2 \times 10^{-9}\text{ A}/\text{cm}^2$, and energy density of $\approx 67\text{ J}/\text{cm}^3$. Dielectric breakdown strength was determined to be $\approx 2.6 \times 10^6\text{ V}/\text{cm}$ by Weibull analysis. These and other results reported here indicate that electronic devices with film-on-foil capacitors would possess higher performance, improved reliability, and enhanced volumetric and gravimetric efficiencies compared with traditional dielectric capacitors.

1. Introduction

With development of green energy technologies and their expanding applications, devices for effectively absorbing, converting, storing, and supplying electrical energy are in increasing demand. Not only high energy storage density but also high-power output is required for many applications. Commercial electrical energy storage and supply devices include fuel cells, batteries, electrochemical supercapacitors, and dielectric capacitors. Among them, fuel cells and batteries exhibit high energy density, but relatively low power density because of the slow movement of charge carriers. Electrochemical supercapacitors offer improved power density at moderate energy density and are promising for many power system applications, but their charge and/or discharge process still requires seconds or tens of seconds. In contrast, dielectric capacitors provide the highest power density because of their extremely high charge/discharge speed. This characteristic makes dielectric capacitors well suited to energy storage applications when high power delivery or uptake is required. However, traditional dielectric capacitors possess low energy density ($\leq 0.1\text{ J}/\text{cm}^3$).

Recently, dielectric film capacitors have attracted increased attention because of their applications as decoupling and DC-link capacitors. They can also be used in AC/DC convertors and in portable power electronics, where the capacitors must be able to operate under high voltage and yet have minimal weight and volume [1-2]. Although high-k oxide film dielectrics exhibit high permittivity and breakdown strength (3 to 12 MV/cm) [3], their dielectric constant is relatively low, and in turn, the volumetric energy density is only in the neighborhood of 1 to 2 J/cm³ [4]. Recently, polymer ferroelectrics, ceramic ferroelectrics, antiferroelectrics, and relaxor ferroelectrics have shown better potential and higher energy density than linear dielectrics [2,5-8]. Chu et al. [2] reported high dielectric breakdown strength and high energy density of $\approx 17\text{ J}/\text{cm}^3$ in the copolymer system poly(vinylidene fluoride-trifluoroethylene) P(VDF-TrFE), where the introduction of defects in this



system converts it to a relaxor ferroelectric with almost negligible remanent polarization. Yao et al. [5] reported relaxor-antiferroelectric thin films, relaxor-ferroelectric thin films, and poly(vinylidene fluoride)-based polymer blend thin films that show high energy density (10 to 25 J/cm³). Ma et al. [6,7] reported energy density of ≈ 53 J/cm³ in antiferroelectric PLZT films grown on metal foils. Hao et al. [8] reported an energy density of ≈ 30 J/cm³ in relaxor ferroelectric PLZT films grown on platinized silicon substrates.

By far, the vast majority of ceramic dielectric films are fabricated on single crystals or silicon wafers [9-11]. Use of metallic substrates, however, is more desirable for the fabrication of large-area devices with low cost. Metal foils coated with ceramic dielectric material, the so-called “film-on-foil dielectric sheets,” can be laminated onto printed circuit boards (PCBs) to create embedded capacitors that have broad applications in power electronics. Alternatively, these film-on-foils could be stacked to form a capacitor cartridge with minimal footprint on a circuit board. However, substantial technical challenges still exist in the fabrication of film-on-foil capacitors that exhibit high dielectric strength and are crack free. Problems include thermal expansion mismatch between films and metal substrates, formation of a low-dielectric-constant parasitic layer at the film/substrate interface, and diffusion of cations from the substrate into the dielectric film.

We earlier reported fabrication of ferroelectric PLZT film-on-foil capacitors on base metal (nickel and copper) sheets [12-14]. To produce film-on-foil sheets with high quality, we have found it necessary to apply a conductive oxide buffer to the nickel foil prior to the deposition of PLZT. This architecture allows crystallization of dielectric ceramic films grown on nickel foils in air without the formation of deleterious interfacial secondary phases [12]. An alternative approach is to process the ceramic dielectric films in a controlled atmosphere with reduced oxygen partial pressure [14]. In this paper, we report our recent results from dielectric characterization under high bias field for PLZT film-on-foil capacitors grown on LNO-buffered nickel substrates.

2. Experiment

High purity (99.98% pure) nickel substrates with dimensions of 25 mm \times 25 mm \times 0.4 mm were obtained from MTI Corp. (Richmond, California). They were polished by chemical-mechanical planarization (CMP). A root-mean-square surface roughness of ≈ 2 nm was measured by atomic force microscopy (AFM) in the tapping mode with 5 μm \times 5 μm scan size. Prior to being coated, CMP-polished nickel substrates were ultrasonically cleaned in distilled water, and then wipe-cleaned with acetone and methanol in sequence.

Prior to the PLZT ($\text{Pb}_{0.92}\text{La}_{0.08}\text{Zr}_{0.52}\text{Ti}_{0.48}\text{O}_3$) deposition, a conductive oxide film of LaNiO_3 (LNO) was coated on the Ni substrate by chemical solution deposition to serve as a buffer layer. LNO precursor solutions with 0.2 M concentration were prepared by dissolving an appropriate amount of lanthanum nitrate hexahydrate and nickel acetate tetrahydrate in 2-methoxyethanol (all from Sigma-Aldrich) and refluxing for 2 h inside a chemical glove box. PLZT precursor solutions with 0.5 M concentration were prepared by a modified 2-methoxyethanol synthesis route [12,15] using an appropriate amount of titanium isopropoxide, zirconium n-propoxide, lead acetate trihydrate, and lanthanum nitrate hexahydrate (all from Sigma-Aldrich). The resulting stock solution contained 20% excess lead to compensate for lead loss during the heat treatments described below. Before being used for coating, the LNO and PLZT precursor solutions were filtered through Restek polytetrafluoroethylene (PTFE) syringe filters (Restek Corp., Bellefonte, PA) with 0.22- μm open pore size. The filtered LNO precursor solution was spin coated with a Laurell WS400 spin processor (Laurell Technologies, North Wales, PA) at 3000 rpm for 30 s on the Ni substrates, pyrolyzed at 450°C for 5 min, and annealed at 625°C for 2-5 min in air. This process was repeated three times to build the desired ≈ 0.4 - μm -thick LNO buffer film. Subsequently, filtered PLZT precursor solution was spin coated on the LNO-buffered Ni substrates at 3000 rpm for 30 s, followed by pyrolysis at 450°C for 5 min and annealing at 650°C for 5-10 min for each coating. After every three layers of coating, additional annealing was performed at 650°C for 15 min. Solution coating and firing were repeated to produce films of desired thickness. All pyrolysis and annealing were performed in air in Lindburg tube furnaces. Each coating resulted in a PLZT film of ≈ 0.115 - μm thickness after pyrolysis and crystallization. Film thickness was determined from cross-sectional images with scanning electron microscopy (SEM) [12]. Phase development in the processed films was studied by a Bruker AXS D8 diffraction system. Film microstructures were characterized by a Hitachi S-4700-II field-emission electron microscope. The grain size and surface roughness were determined by a Veeco Instruments D3100 scanning probe microscope operated in the tapping mode.

Platinum (Pt) top electrodes with thickness of 100 nm were deposited by electron-beam evaporation through a shadow mask to define ≈ 250 - μm -diameter capacitors. Samples with Pt top electrodes were annealed at 450°C in air for 2 min for electrode conditioning. A Signatone QuieTemp® probe system with heatable vacuum chuck (Lucas Signatone Corp., Gilroy, CA) was used for electrical characterization. For the electrical measurements, the Pt/PLZT/LNO/Ni heterostructure was contacted by a Pt top electrode pad with one probe and the substrate

(bottom electrode) with the other. A positive applied voltage corresponds to a configuration where the top electrode is at a higher potential than the bottom electrode. An Agilent E4980A precision LCR meter was used to determine the capacitance and dissipation factor under an applied bias field. A Radiant Technologies Precision Premier II tester measured the hysteresis loops. The capacitor samples were immersed in Fluka silicone oil (Sigma-Aldrich) during measurements of high-field hysteresis loops and dielectric breakdown. A Keithley 237 high-voltage source meter measured the current-voltage characteristics. The leakage current density was determined by fitting the current density relaxation data to the Curie-von Schweidler equation [16].

3. Results and discussion

Figure 1 shows the X-ray diffraction (XRD) pattern measured on a PLZT film deposited on LNO-buffered Ni substrate. The diffraction pattern indicates that PLZT film is well crystallized and exhibits no preferred crystallographic orientation. The PLZT films exhibit a perovskite structure with tetragonal distortion (JCPDS No. 56-0900). Peaks from LNO buffer and nickel substrate are also visible on the diffraction pattern. No crack or delamination was observed from SEM [12]. As shown in the Fig. 1 inset, the PLZT film has an average grain size of ≈ 45 nm as determined from atomic force microscopy (AFM).

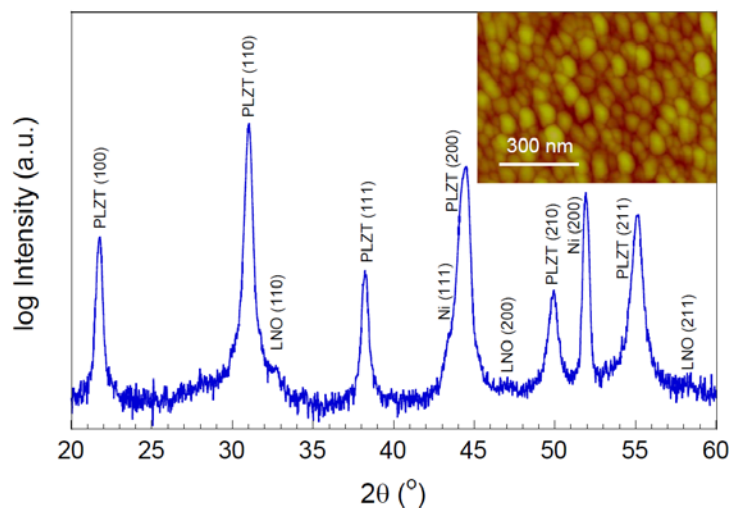


Fig. 1. X-ray diffraction pattern and AFM image (inset) of ≈ 2 - μ m-thick PLZT film deposited by chemical solution deposition on LNO-buffered nickel substrate.

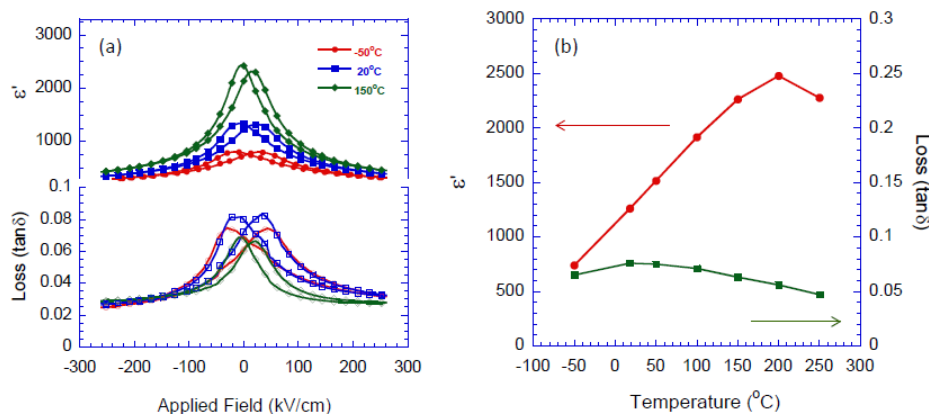


Fig. 2. Dielectric properties as function of (a) applied field and (b) temperature for PLZT film-on-foil capacitor.

Figure 2a shows the dielectric constant (relative permittivity) and loss as a function of applied bias field at three temperatures on a PLZT film grown on LNO-buffered nickel substrate. At zero applied field, we measured dielectric constant of ≈ 700 and dielectric loss of ≈ 0.06 at -50°C , dielectric constant of ≈ 1300 and loss of ≈ 0.07 at 20°C , and dielectric constant of ≈ 2200 and dielectric loss of ≈ 0.05 at 150°C . The dielectric constant increases while dielectric loss decreases with increasing temperature. At 200°C , we measured a dielectric constant of 2500 and loss of ≈ 0.05 . Both dielectric constant and loss decrease with applied bias field. A dielectric tunability, $1 - \varepsilon'(E)/\varepsilon'(0)$, of $\approx 55\%$ was measured at field of 100 kV/cm. Figure 2b shows the dielectric properties of a

PLZT/LNO/Ni sample measured within the temperature range between -50 and 250°C . The dielectric constant increases while the dissipation factor decreases with increasing temperature from room temperature to 200°C . Maxima of the dielectric constant and dissipation factor occurred at $\approx 200^{\circ}\text{C}$ and room temperature, respectively.

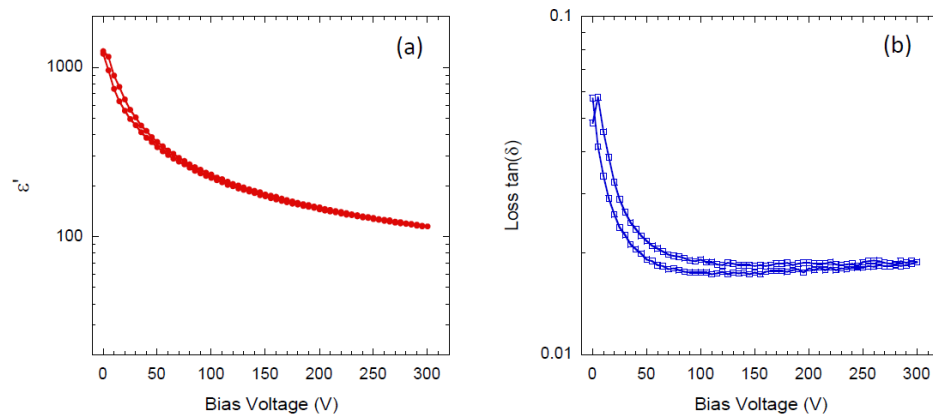


Fig. 3. Bias voltage dependency of (a) dielectric constant and (b) loss tangent of PLZT/LNO/Ni film-on-foil capacitor at room temperature and 10 kHz.

Figure 3 shows dielectric constant and loss measured at room temperature and 10 kHz under bias voltage up to 300 V. We measured a dielectric constant of ≈ 110 and dielectric loss ≈ 0.02 under applied bias voltage of 300 V. This PLZT film of $\approx 2\text{-}\mu\text{m}$ thickness was subjected to a bias field of $\approx 1.5 \times 10^6 \text{ V/cm}$ when a 300-V bias voltage was applied. The charging and discharging curves nearly overlay under high bias. The dielectric constant decreases steadily with increasing bias field because of the ferroelectric nature of the PLZT film. Because dipole movement is clamped under high bias field [17], the apparent dielectric constant is depressed with increased field. The dielectric loss drops rapidly under applied bias voltage up to $\approx 50 \text{ V}$; and it remains nearly constant at ≈ 0.02 with further increase in bias voltage.

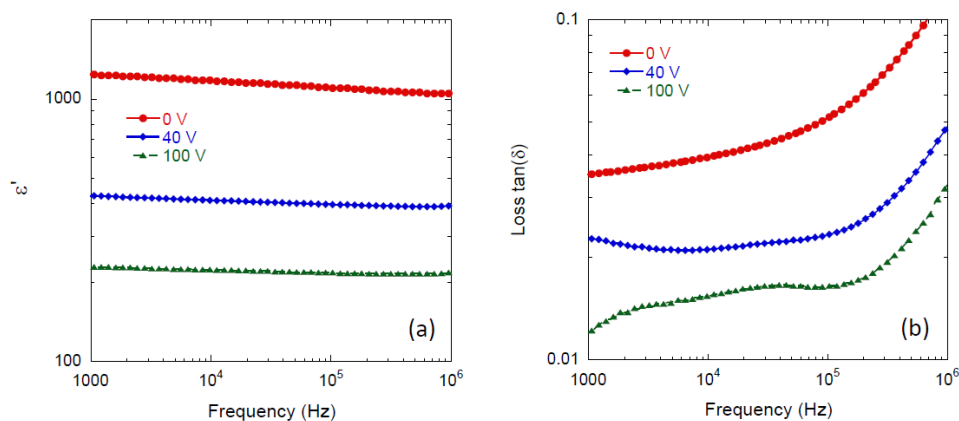


Fig. 4. Frequency dependency of (a) dielectric constant and (b) loss tangent for PLZT/LNO/Ni film-on-foil capacitor under different bias voltages at room temperature.

Figure 4 shows the dielectric constant and dielectric loss measured as a function of frequency under various applied bias voltages up to 100 V. The dielectric constant decreases slightly while the dielectric loss increases substantially with increasing frequency. At 100 kHz under 100 V bias, we measured a dielectric constant of ≈ 220 and dielectric loss ≈ 0.02 at room temperature.

Figure 5 shows polarization-electric field (P-E) hysteresis loops of a $\approx 2\text{-}\mu\text{m}$ -thick PLZT grown on LNO-buffered nickel foil measured with sweeping frequency of 100 Hz under low and high applied field conditions. From the P-E hysteresis loop, we measured remanent polarization $P_r = 25.7 \text{ }\mu\text{C/cm}^2$ and coercive field $E_c = 28.9 \text{ kV/cm}$, as shown in Fig. 5a. From the high-field hysteresis loop, we measured a recoverable energy density of $\approx 67 \text{ J/cm}^3$ with a maximum applied voltage of 800 V (corresponding to an applied field of $\approx 4.0 \times 10^6 \text{ V/cm}$), as shown in Fig. 5b. The ratio of recoverable energy to input energy is $\approx 75\%$.

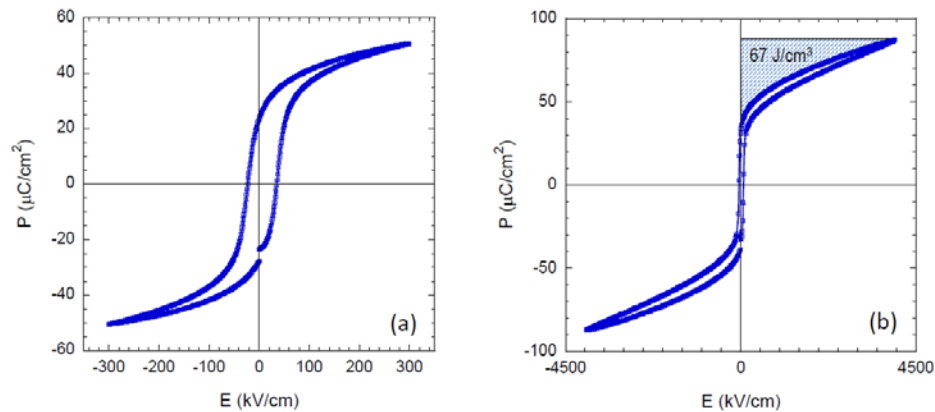


Fig. 5. P-E hysteresis loops for PLZT/LNO/Ni film-on-foil capacitor measured with (a) low field up to 60 V and (b) high field up to 800 V.

Figure 6 shows P_r and E_c measured as a function of temperature with low field condition. Both P_r and E_c decrease steadily with increasing temperature. We measured $P_r = 25.7 \mu\text{C}/\text{cm}^2$ and $E_c = 28.9 \text{ kV}/\text{cm}$ at room temperature, as well as $P_r = 7.5 \mu\text{C}/\text{cm}^2$ and $E_c = 8.2 \text{ kV}/\text{cm}$ at 200°C , for a $\approx 2\text{-}\mu\text{m}$ -thick PLZT film grown on LNO-buffered nickel foil.

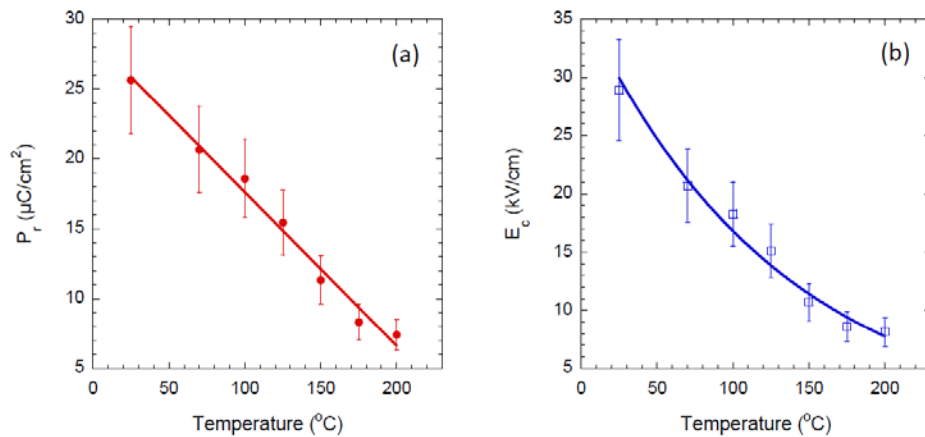


Fig. 6. Temperature-dependent (a) remanent polarization and (b) coercive field of PLZT/LNO/Ni film-on-foil capacitor.

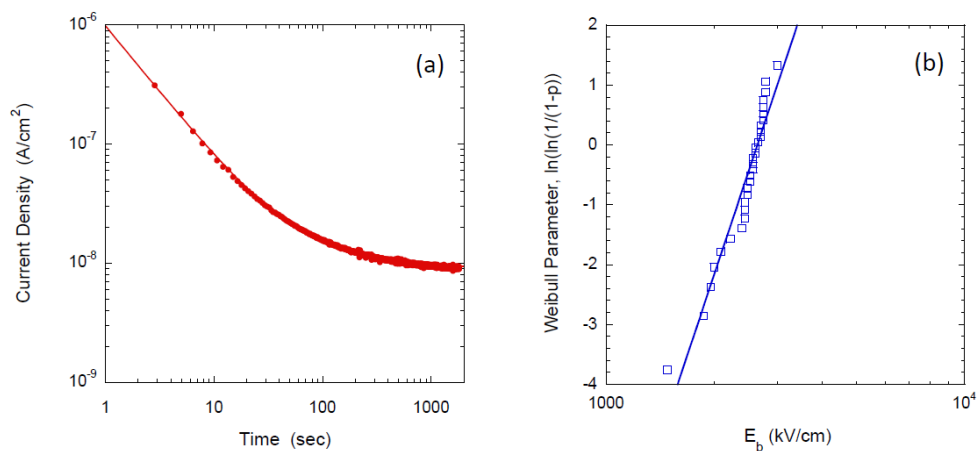


Fig. 7. (a) Time-relaxation current density and (b) Weibull plot measured on PLZT/LNO/Ni film-on-foil capacitor at room temperature.

Figure 7a shows the time relaxation for the current density measured at room temperature on PLZT/LNO/Ni with a constant bias field of ≈ 100 kV/cm across the top and bottom electrodes. The measurements were conducted by keeping the top Pt electrode positive and the bottom Ni electrode grounded. The relaxation curve shows strong initial time dependence. Fitting data to the Curie-von Schweidler law [16], we determined steady-state leakage current densities of $\approx 9.2 \times 10^{-9}$ A/cm² for ≈ 2 - μ m-thick PLZT grown on LNO/Ni substrate. Figure 7b shows the Weibull plot of breakdown field strength obtained at room temperature from 30 capacitor samples of PLZT grown on LNO/Ni substrates. The solid straight line is a least-square fitting to the two-parameter distribution function [18,19]. We measured mean breakdown field of 2.6×10^6 V/cm and Weibull modulus β of 7.8 for ≈ 2 - μ m-thick PLZT grown on LNO/Ni substrates.

4. Conclusions

We have grown high-breakdown-strength ferroelectric PLZT films on LNO-buffered Ni foils by chemical solution deposition. X-ray diffraction revealed that the PLZT films are well crystallized after heat treatment at 650°C. The dielectric constant increases while the dielectric loss decreases with increasing temperature from room temperature to 200°C. We measured dielectric constant of ≈ 700 and loss of ≈ 0.06 at -50°C, dielectric constant of ≈ 1300 and loss of ≈ 0.07 at 20°C, and dielectric constant of ≈ 2200 and loss of ≈ 0.05 at 150°C, respectively. Hysteresis measurement revealed that both remanent polarization P_r and coercive field E_c decrease with increasing temperature. We measured P_r of ≈ 26 μ C/cm² and E_c of ≈ 29 kV/cm at 20°C, and P_r of ≈ 7.5 μ C/cm² and E_c of ≈ 8.2 kV/cm at 200°C. Steady-state leakage current densities of $\approx 9.2 \times 10^{-9}$ A/cm², mean breakdown field of $\approx 2.6 \times 10^6$ V/cm, and energy density of ≈ 67 J/cm³ were measured at room temperature.

Acknowledgment

This work was funded by the U.S. Department of Energy, Vehicle Technologies Program, under Contract DE-AC02-06CH11357.

References

- [1] S. A. Sherrill, P. Banerjee, G. W. Rubloff, and S. B. Lee, *Phys. Chem. Chem. Phys.* **13** (2011) 20714.
- [2] B. Chu, X. Zhou, K. Ren, B. Neese, M. Lin, Q. Wang, F. Bauer, and Q. M. Zhang, *Science* **313** (2006) 334.
- [3] J. W. McPherson, J. Kim, A. Shanware, H. Mogul, and J. Rodriguez, *IEEE Trans. Electron Dev.* **50** (2003) 1771.
- [4] N. Ortega, A. Kumar, J. F. Scott, D. B. Chrisey, M. Tomazawa, S. Kumari, D. G. B. Diestra, and R. S. Katiyar, *J. Phys.: Condens. Matter* **24** (2012) 445901.
- [5] K. Yao, S. Chen, M. Rahimabady, M. S. Mirshekarloo, S. Yu, F. E. H. Toy, T. Sritharan, and L. Lu, *IEEE Trans. Ultrason. Ferroelectr. Freq. Control* **58** (2011) 1968.
- [6] B. Ma, D. K. Kwon, M. Narayanan, U. Balachandran, *Mater. Res. Bull.* **44** (2009) 11.
- [7] B. Ma, D. K. Kwon, M. Narayanan, U. Balachandran, *J. Mater. Res.* **24** (2009) 2993.
- [8] X. Hao, Y. Wang, J. Yang, S. An, and J. Xu, *J. Appl. Phys.* **112** (2012) 114111.
- [9] H.-J. Zhao, T.-L. Ren, N.-X. Zhang, R.-Z. Zuo, X.-H. Wang, L.-T. Liu, Z.-J. Li, Z.-L. Gui, and L.-T. Li, *Mater. Sci. Eng. B* **99** (2003) 195.
- [10] L. B. Kong and J. Ma, *Mater. Lett.* **56** (2002) 30.
- [11] S. Chao, B. Ma, S. Liu, M. Narayanan, and U. Balachandran, *Mater. Res. Bull.* **47** (2012) 907.
- [12] B. Ma, D. K. Kwon, M. Narayanan, and U. Balachandran, *J. Electroceram.* **22** (2009) 383.
- [13] U. Balachandran, D. K. Kwon, M. Narayanan, and B. Ma, *J. Europ. Ceram. Soc.* **30** (2010) 365.
- [14] M. Narayanan, B. Ma, and U. Balachandran, *Mater. Lett.* **64** (2010) 22.
- [15] Q. Zou, H. E. Ruda, and B. G. Yacobi, *Appl. Phys. Lett.* **78** (2001) 1282.
- [16] K. Jonscher, *Dielectric Relaxation in Solids*, Chelsea Dielectrics Press, London (1983).
- [17] B. Ma, Z. Hu, S. Liu, M. Narayanan, and U. Balachandran, *Appl. Phys. Lett.* **102** (2013) 072901.
- [18] W. Weibull, *J. Appl. Mech.* **18** (1951) 293-297.
- [19] L. A. Dissado, *J. Phys. D: Appl. Phys.* **23** (1990) 1582.